Synchronization in Coupled Laser Arrays with Correlated and Uncorrelated Disorder

Amit Pando, Sagie Gadasi, Eran Bernstein, Nikita Stroev, Asher Friesem, and Nir Davidson
Department of Physics of Complex Systems, Weizmann Institute of Science, Rehovot 7610001, Israel

(Received 17 December 2023; accepted 8 July 2024; published 9 September 2024)

The effect of quenched disorder in a many-body system is experimentally investigated in a controlled fashion. It is done by measuring the phase synchronization (i.e., mutual coherence) of 400 coupled lasers as a function of tunable disorder and coupling strengths. The results reveal that correlated disorder has a nontrivial effect on the decrease of phase synchronization, which depends on the ratio of the disorder correlation length over the average number of synchronized lasers. The experimental results are supported by numerical simulations and analytic derivations.

DOI: 10.1103/PhysRevLett.133.113803

Introduction—Many different quantum and classical physical systems can be described by the framework of many-body interacting oscillators. Examples include transverse-field spin models, wherein spins rotating around a local magnetic field can synchronize to reach finite magnetization even in the presence of a spatially varying magnetic field [1–5]. Synchronization of classical phase oscillators has been studied for decades through the Kuramoto model [6], and is manifested in many different systems such as arrays of Josephson junctions [7,8], coupled laser arrays [9,10], and even human networks [11]. In all of these, disorder plays a major role in synchronization. There are cases where disorder leads to synchronization [12,13], but in general it acts as an obstacle, preventing the interaction between the individual members of the ensemble so they cannot synchronize.

While many theoretical investigations of the effects of disorder on synchronization have been performed [6,14–17], it is difficult to verify the results experimentally because excessively high control and accuracy are needed. Several systems with robustness to disorder were recently reported [18–23], but with limited ability to tune the disorder and quantify their robustness.

In this work, we resort to an array of 400 lasers with nearest-neighbor coupling and well-controlled quenched (time-independent) disorder to obtain a tunable system for investigating the effects of disorder on synchronization (locking) of their optical phase. The disorder is introduced in the form of frequency detuning, where the resonant frequency of each individual laser is shifted. By precisely controlling the magnitude of the disorder, we show how it gradually diminishes the ability of the lasers to synchronize. By varying spatial properties of the disorder, we demonstrate how its effects depend on a nontrivial interplay between the scales of the problem, namely, the correlation length of the disorder and the average number of synchronized lasers, in good agreement with our numerical and theoretical derivations.

Our experimental system of coupled laser arrays can be readily extended to investigate the effects of controlled disorder on topological states [19,24,25], non-Hermitian dynamics [26,27], geometric frustration [28], spin simulators, and physical solvers for complex problems [29–32].

Experimental system—Our experimental system, schematically shown in Fig. 1 and described in detail in [33] is comprised of a digital degenerate cavity laser (DDCL) [34–36]. It includes an intracavity 4f telescope, a 98% reflectivity output coupler, a 3 mm thick ND:YVO4 gain medium lasing at wavelength $\lambda = 1.06$ μm, a reflective

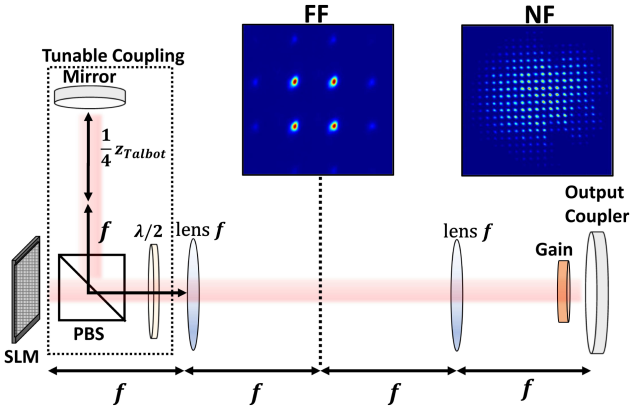

FIG. 1. Experimental system. A modified digital degenerate cavity laser [34–36] with an intracavity SLM that defines 400 lasers (20 × 20 square lattice) with a normally distributed random frequency detuning pattern having standard deviation $\tau_c\Omega_{\mathrm{rms}}$ and correlation length ξ. The tunable coupling arrangement (surrounded by the dashed lines) introduces Talbot coupling [37,38] between nearest neighbor lasers whose strength can be continuously tuned by rotating the $\lambda/2$ wave plate. The insets show representative far-field (left) and near-field (right) intensity distributions for zero disorder strength ($\tau_c\Omega_{\mathrm{rms}} = 0$). The four sharp diffraction FF peaks indicate near-perfect phase synchronization with π phase difference between neighbors due to negative coupling.

spatial light modulator (SLM) with pixel size of 8 = μm, and a tunable coupling arrangement. The gain medium has a fluorescence lifetime of $\tau_f \approx 100$ μs, and is end- pumped by a 808 nm diode laser with a pulse duration of 500 μs at 4 Hz repetition rate. The intracavity SLM forms a digital amplitude and phase mask, to form 400 independent lasers in a 20×20 square array with spacing between adjacent lasers of $d_{\mathrm{lat}} = 300$ μm, (see NF inset in Fig. 1) and to precisely control the frequency detuning between the lasers. By changing the phase retardation of each SLM pixel, we locally vary the effective cavity length with a precision of $(\lambda/256)$ and thereby detune the resonant frequency of each laser with a precision of $\tau_c \Delta\Omega = (2\pi/256)$ rad, where $\tau_c = (2l/c) \approx 13.3$ ns is the cavity round-trip time. The 200 μm diameter of each site in the array ensures a single Gaussian spatial mode for each laser.

Intracavity polarizing beam splitter (PBS) and $\lambda/2$-waveplate deflect a controllable amount of the light into a second branch of the cavity [39–41] where the lasers are Talbot coupled [37,38]. This provides a tunable coupling strength of $K_{\max}\sin^2(2\theta)$ between nearest neighbor lasers [33], where θ is the rotation angle of the $\lambda/2$ waveplate and $K_{\max} \approx -0.45$ is the calculated full Talbot coupling strength [37,38].

In each experimental realization, the SLM was controlled to obtain a normally distributed random frequency detuning pattern with a standard deviation Ω_{rms} and a Gaussian spatial correlation function with a waist that we refer to as ξ, the correlation length of the frequency detuning pattern. Hence, the correlation of the frequency detuning between the lasers in sites (i, j) and (i', j') is

$$\langle \Omega_{ij}\Omega_{i'j'}\rangle = (\Omega_{\mathrm{rms}})^2 e^{-\frac{(i-i')^2+(j-j')^2}{\xi^2}}. \tag{1}$$

Equation (1) indicates that as ξ increases, the detunings of neighboring lasers are more likely to be similar. To provide near-perfect starting conditions for our experiments we first apply intracavity adaptive optics [33] to reduce aberrations and uncontrolled frequency detuning (see below and Supplemental Material [42], Fig. S2).

For each realization, we pump the laser and measure the resulting steady state near field (NF) and far field (FF) intensity distributions. The measured distributions are averaged over 50 random realizations for each value of $\tau_c\Omega_{\mathrm{rms}}$ and ξ. The inital pump power was $P = 19.8W \approx 4P_{\mathrm{th}}$, and increased as required to compensate for the increased losses due to the introduced disorder (see Fig. S1 in [42]). The FF intensity distribution (I_{FF}) is proportional to the Fourier transform of the coherence function of the electric field [43,44]. We thus use the average FF inverse participation ratio (IPR) as the synchronization order parameter:

$$\mathrm{IPR} = \frac{\int\int \mathrm{d}x\mathrm{d}y I_{\mathrm{FF}}^2}{(\int\int \mathrm{d}x\mathrm{d}y I_{\mathrm{FF}})^2}. \tag{2}$$

The IPR is a common measure of localization in distributions and is correlated with the average number of synchronized (i.e., mutually coherent) lasers (see Fig. S4 in [42]) [33,44–46]. For an array of lasers, each with a single Gaussian mode, and with a mutual coherence length l_c, IPR $\propto l_c^2 \equiv A_c$. We interpret A_c as a coherence area and $N = A_c/d_{\mathrm{lat}}^2$ as the average number of synchronized (mutually coherent) lasers [42]. The proportionality constants are determined by the geometry of the system, and remain constant throughout the experiments. In earlier investigations we found that the results of the IPR measurements of the laser array coherence were equivalent to interferometric phase measurements or spectral frequency measurements, while being simpler and more reliable for large and disordered arrays [40,47,48].

Results, uncorrelated disorder—Figure 2 shows the experimental normalized FF IPR as a function of the applied disorder strength (normalized to the coupling strength) $\tau_c\Omega_{\mathrm{rms}}/|K|$, for uncorrelated ($\xi = 0$) normally distributed frequency detuning patterns. As evident, increasing the disorder leads to a monotonic decrease in the IPR and deterioration of synchronization, as manifested by the significant broadening of the FF intensity peaks, shown in the insets (see also Fig. S4 in [42]). Results for different $|K|$ agree well with each other, with the IPR dropping to half for $\tau_c\Omega_{\mathrm{rms}}/|K| \approx 0.81(7)$, attesting that synchronization is determined by the ratio $\tau_c\Omega_{\mathrm{rms}}/|K|$.

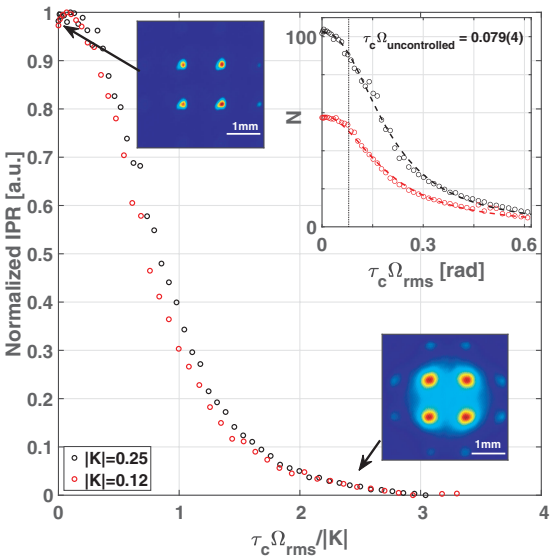

FIG. 2. Experimental normalized FF IPR as a function of the ratio of disorder over the coupling strength, $\tau_c\Omega_{\mathrm{rms}}/|K|$ for two coupling values. Insets show the average FF intensity distribution at $\tau_c\Omega_{\mathrm{rms}}/|K| = 0$ and 2.48 for coupling strength $|K| = 0.25$. Top right inset: Average number of synchronized lasers, $N \equiv A_c/d_{\mathrm{lat}}^2$, as a function of disorder. Dashed curves denote best fits to $N = \{a/[(\tau_c\Omega_{\mathrm{rms}})^b + c]\}$, and the dotted vertical line denotes the estimated value of $\tau_c\Omega_{\mathrm{rms,uncontrolled}} = 0.079$ rad.

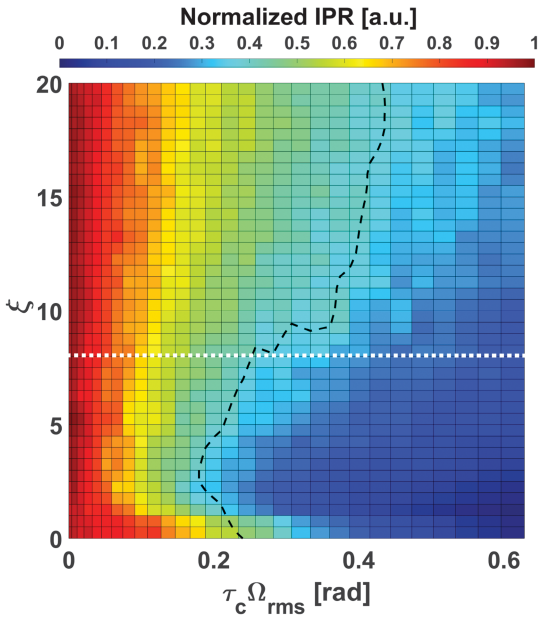

FIG. 3. Measured FF IPR as a function of the disorder strength $\tau_c\Omega_{\mathrm{rms}}$ and its correlation length ξ for $|K| = 0.25$. The black dashed curve denotes IPR $= 0.4$, indicating the nonmonotonic dependence on ξ. The white dotted line is along $\xi = 8$ (detailed in Fig. 4).

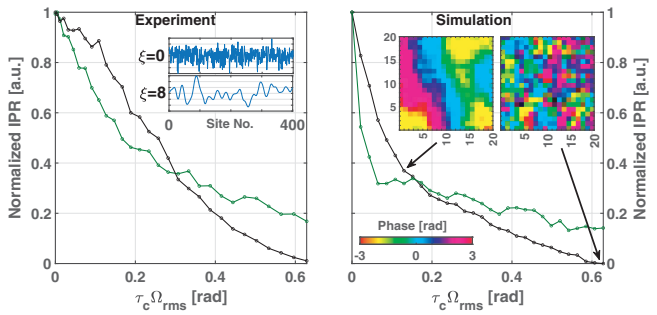

FIG. 4. Experimental and numerically simulated normalized FF IPR as a function of disorder $\tau_c\Omega_{\mathrm{rms}}$ for uncorrelated disorder $\xi = 0$ (black) and for correlated disorder with $\xi = 8$ (green). Inset, left: Representative realizations of disorder vectors with the same length (400 sites) and $\tau_c\Omega_{\mathrm{rms}}$ for $\xi = 0$ and $\xi = 8$. Inset, right: Examples of synchronized lasers in LRE simulations for uncorrelated disorder ($\xi = 0$) with $\tau_c\Omega_{\mathrm{rms}} = 0.15, 0.62$ rad. Each pixel represents the phase of the corresponding laser in the array. Additional examples are provided in Fig. S3 in [42].

The top right inset in Fig. 2 shows that the average number of synchronized lasers (determined from the FF intensity distribution [33,44]) is also reduced monotonically with $\tau_c\Omega_{\mathrm{rms}}$. Note that N differs significantly for the two different coupling strengths for small $\tau_c\Omega_{\mathrm{rms}}$ due to the uncontrolled disorder in our system.

Fitting the data from Fig. 2 top right inset to $N = \{a/[(\tau_c\Omega_{\mathrm{rms}})^b + c]\}$ we obtain $b = 2.3(1)$, $2.0(1)$ for $|K| = 0.25$, 0.12, respectively. These results are in good agreement with the theoretical value of $b = 2$ in Eq. (5) which we consider in the last section of this Letter. We identify c as a manifestation of our uncontrolled disorder $(\tau_c\Omega_{\mathrm{rms,uncontrolled}})^b = c$, to estimate $\tau_c\Omega_{\mathrm{rms,uncontrolled}} \approx 0.079(4)$ rad.

Results, correlated disorder—We now consider the effects of correlated disorder ($\xi > 0$) on synchronization. The results for $|K| = 0.25$ are presented in Figs. 3–5 (see additional results in Figs. S5–S7 in [42]). Figure 3 shows the experimental normalized IPR of the measured FF intensity distribution as a function of $\tau_c\Omega_{\mathrm{rms}}$ and ξ. All measured IPR values were normalized such that IPR $= 1, 0$ are the maximal and minimal values measured across all experiments, respectively. For all values of ξ, the IPR monotonically decreases as $\tau_c\Omega_{\mathrm{rms}}$ is increased, as expected. However, the IPR dependence on ξ is nontrivial and nonmonotonic.

Figure 4 shows the experimental normalized and calculated IPR as a function of $\tau_c\Omega_{\mathrm{rms}}$ for uncorrelated disorder ($\xi = 0$) and correlated disorder with $\xi = 8$. For weak disorder $\tau_c\Omega_{\mathrm{rms}} < 0.31$ rad, the IPR is lower (worse synchronization) for the correlated disorder, while for strong disorder, the opposite is true. Numerical simulation of the full laser rate equations [49] (see procedure in [42]) are in good agreement with the experimental results and validate the nonmonotonic dependence on ξ.

This nonmonotonicity is again seen in Fig. 5 that shows the experimental and calculated normalized IPR as a function of ξ for different values of $\tau_c\Omega_{\mathrm{rms}}$. In the case of strong disorder (purple), the IPR monotonically increases with ξ. However, for weak disorders the dependence on ξ is nonmonotonic, and the IPR reaches a minimum at an intermediate value of ξ that decreases with the strength of the disorder. It is apparent that there is a good agreement between the experimental and simulation results.

Analysis and discussion—To elucidate our experimental and simulation results, we consider a toy model that is based on the Kuramoto model [6], which can describe the dynamics of coupled lasers when their intensities are

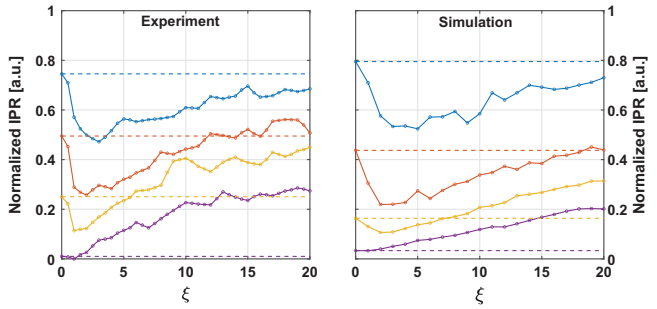

FIG. 5. Experimental and numerically simulated normalized FF IPR as a function of correlation length ξ for different values of disorder, $\tau_c\Omega_{\mathrm{rms}} = 0.12, 0.23, 0.36, 0.62$ rad (blue, orange, yellow, and purple, respectively). Dashed lines show the corresponding IPR values for $\xi = 0$ for reference.

identical and high above threshold [28,50]. Theoretical studies of models with nearest neighbor coupling have shown that for any finite frequency detuning Ω_i (taking $\tau_c = 1$), the oscillators synchronize in local clusters, where the maximal number of synchronized oscillators in a single cluster is bounded [6,51,52].

Specifically, we consider a one-dimensional chain of Kuramoto oscillators with bidirectional nearest neighbor coupling as a toy model of our system. We chose to work with a one-dimensional theoretical system for which analytical solutions exist (rather than the two-dimensional system in our experiments and simulations where analytical solutions do not exist). Although it is not obvious that results from a one-dimensional system can be applied to a two-dimensional one, theoretical studies that suggest that the conditions for existence of the phase locked state of the system and its properties are similar for one- and two-dimensional systems [51,52]. We found that our limited toy model provides some insight into the results of our two-dimensional system, and shows similar qualitative behavior to that which we have observed in experiments.

For a one-dimensional chain of oscillators with nearest neighbor coupling, the necessary condition for synchronization of N oscillators is that the maximal accumulated detuning along the N oscillators must be smaller than the coupling strength K between two neighbors [51]:

$$\max_{1\le j\le N}|X_j| \le K \tag{3}$$

with X_j being the accumulated detuning

$$X_j = \sum_{i=1}^{j}\Omega_i - \frac{1}{N}\left(\sum_{i=1}^{N}\Omega_i\right). \tag{4}$$

K_c, the critical required coupling for synchronization of N oscillators is thus simply $\max|X_j|$. When Ω_j has a normal distribution (i.e., for uncorrelated disorder), Eq. (3) describes the maximal displacement of a random walker, $\max|X_j| \propto \Omega_{\mathrm{rms}}\sqrt{N}$, such that the synchronized cluster size is

$$N \propto \frac{K^2}{\Omega_{\mathrm{rms}}^2}. \tag{5}$$

Equation (5) agrees well with the results presented in Fig. 2, as well as the fit to the experimental data.

We now extend our model for the case of correlated quenched disorder. Figure 6 (upper left) shows $\langle\max|X_j|\rangle = K_c$ numerically calculated from Eq. (4) as a function of the synchronized cluster size N for Gaussian detuning disorder of $\Omega_{\mathrm{rms}} = 1$ and several correlation lengths ξ (the brackets indicate an average over different disorder realizations). For small synchronized cluster sizes K_c decreases with ξ, while for larger cluster sizes, K_c increases with ξ. Notably, the crossing point between the two trends is roughly at $N \sim \xi$.

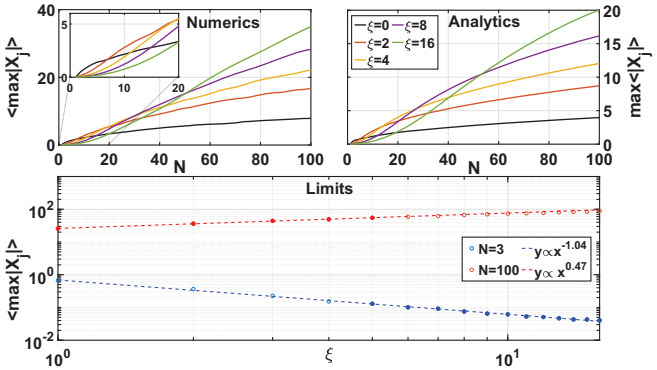

FIG. 6. The maximal accumulated detuning $\max\langle|X_j|\rangle$ as a function of the number of oscillators N and disorder correlation length ξ. Upper left: Numerical integration of Eq. (4) averaged over 100 random realizations. The inset shows a magnified view for low N values. Upper right: Corresponding analytical evaluation using Eq. (6). Bottom: Log-log plot of the numerical data as a function of ξ for $N = 100$ (red) and $N = 3$ (blue) N. Linear fits to the colored-in points (dashed lines) yield good agreement of the ξ scaling to the limiting analytical approximations.

The result of Eq. (4) in the case of correlated disorder can be approximated analytically (see derivation in [42]) as

$$\langle|X_j|\rangle^2 \approx \Omega_{\mathrm{rms}}^2\frac{\pi\xi L}{8}\frac{1}{\frac{\xi}{\sqrt{2\pi}}\left(e^{-\frac{2L^2}{\xi^2}}-1\right)+L\,\mathrm{erf}\left(\frac{\sqrt{2}L}{\xi}\right)} \times\sum_{i=0}^{L}\left[\mathrm{erf}\left(\frac{j-i}{\xi}\right)+\frac{1}{2}e^{-\frac{(j-i)^2}{\xi^2}}-\frac{j}{N}\left(\mathrm{erf}\left(\frac{N-i}{\xi}\right)+\frac{1}{2}e^{-\frac{(N-i)^2}{\xi^2}}\right)+\left(1-\frac{j}{N}\right)\left(\mathrm{erf}\left(\frac{i}{\xi}\right)-\frac{1}{2}e^{-\frac{i^2}{\xi^2}}\right)\right]^2. \tag{6}$$

The analytic approximations of Eq. (6) shown in Fig. 6 (upper right) are in good agreement with the exact numerical integration of Eq. (4) (Fig. 6 upper left) and validate the nonmonotonic dependence of K_c on ξ and the cluster size.

Analyzing the limiting behavior of Eq. (6) reveals two distinct regimes. In one regime where $N \gg \xi$, $\max\langle|X_j|\rangle \to \sqrt{\xi N}$, equivalent to the displacement of a random walker with a step size $\xi > 1$. In the other regime, $N \ll \xi$, $\max\langle|X_j|\rangle \to (N^2/\xi)$, which can also be derived directly from Eq. (3) by treating the applied disorder as a long wavelength perturbation $\Omega_i = \sin(i/\xi)$. A log-log linear fit to the numerically evaluated $\langle\max|X_j|\rangle$ as a function of ξ is shown in Fig. 6 (bottom) for $N = 3$ and $N = 100$. Both regimes are well fitted by $y = ax^b$ with $b = -1.04(6), 0.47(4)$ for the $\xi \gg N$, $\xi \ll N$ regimes, in good agreement with the theoretical limiting behavior of

$b = -1$, 0.5, respectively. The results from the analytical toy model reveal a behavior which is qualitatively similar to the nonmonotonic relationship between the disorder parameters $\tau_c\Omega_{\mathrm{rms}}, \xi$ and the synchronization of the array shown in Figs. 3–5.

Conclusions—We experimentally investigated the effects of quenched disorder on the synchronization of coupled oscillators by means of frequency detuning disorder in coupled laser arrays. Our results demonstrate how increased disorder results in a gradual deterioration in synchronization that depends on the ratio of the coupling strength over the disorder strength. Our experimental results are supported by both numerical simulations and an analytic toy model. In addition, we found that the correlated disorder can either improve or degrade synchronization compared to uncorrelated disorder, depending on the ratio of its correlation length ξ and the average number of synchronized lasers N: For $\xi \ll N$, $N \propto (K^2/\xi^2\Omega_{\mathrm{rms}}^2)$ revealing the behavior of a correlated random walker. In contrast, disorder with $\xi \gg N$ is effectively a low frequency perturbation along the cluster and thus causes a smaller decay in synchronization to yield $N \propto \sqrt{(\xi K/\Omega_{\mathrm{rms}})}$.

Our results provide insight into the effects and management of disorder that can be exploited to improve systems where disorder has an inherent correlation time or length (e.g., spin and photonic systems). By controlling the applied disorder, it should be possible to quantify protection against disorder by means of topological effects [18–23], and study the effects of disorder on spin simulators and solvers which are based on coupled lasers or parametric oscillators [29–31].

Acknowledgments—The authors wish to acknowledge The Israel Science Foundation (Grant No. 1520/20), the Joint NSFC-ISF Research Grant (Grant No. 3652/21), and the Minerva Foundation for their support.

[1] T. G. Kiely and J. K. Freericks, Relationship between the transverse-field Ising model and the xy model via the rotating-wave approximation, Phys. Rev. A **97**, 023611 (2018).
[2] M. Henkel, Statistical mechanics of the 2D quantum xy model in a transverse field, J. Phys. A **17**, L795 (1984).
[3] R. Juhász, I. A. Kovács, and F. Iglói, Random transverse-field Ising chain with long-range interactions, Europhys. Lett. **107**, 47008 (2014).
[4] R. H. McKenzie, Exact results for quantum phase transitions in random xy spin chains, Phys. Rev. Lett. **77**, 4804 (1996).
[5] D. S. Fisher, Random transverse field Ising spin chains, Phys. Rev. Lett. **69**, 534 (1992).
[6] J. A. Acebrón, L. L. Bonilla, C. J. P. Vicente, F. Ritort, and R. Spigler, The Kuramoto model: A simple paradigm for synchronization phenomena, Rev. Mod. Phys. **77**, 137 (2005).
[7] K. Wiesenfeld, P. Colet, and S. H. Strogatz, Frequency locking in Josephson arrays: Connection with the Kuramoto model, Phys. Rev. E **57**, 1563 (1998).
[8] B. R. Trees, V. Saranathan, and D. Stroud, Synchronization in disordered Josephson junction arrays: Small-world connections and the Kuramoto model, Phys. Rev. E **71**, 016215 (2005).
[9] M. K. S. Yeung and S. H. Strogatz, Time delay in the Kuramoto model of coupled oscillators, Phys. Rev. Lett. **82**, 648 (1999).
[10] N. Takemura, K. Takata, M. Takiguchi, and M. Notomi, Emulating the local Kuramoto model with an injection-locked photonic crystal laser array, Sci. Rep. **11**, 8587 (2021).
[11] S. Shahal, A. Wurzberg, I. Sibony, H. Duadi, E. Shniderman, D. Weymouth, N. Davidson, and M. Fridman, Synchronization of complex human networks, Nat. Commun. **11**, 3854 (2020).
[12] A. Niederberger, M. M. Rams, J. Dziarmaga, F. M. Cucchietti, J. Wehr, and M. Lewenstein, Disorder-induced order in quantum xy chains, Phys. Rev. A **82**, 013630 (2010).
[13] J. Villain, R. Bidaux, J.-P. Carton, and R. Conte, Order as an effect of disorder, J. Phys. **41**, 1263 (1980).
[14] B. Sonnenschein and L. Schimansky-Geier, Approximate solution to the stochastic Kuramoto model, Phys. Rev. E **88**, 052111 (2013).
[15] E. Granato and J. M. Kosterlitz, Quenched disorder in Josephson-junction arrays in a transverse magnetic field, Phys. Rev. B **33**, 6533 (1986).
[16] V. Vlasov and A. Pikovsky, Synchronization of a Josephson junction array in terms of global variables, Phys. Rev. E **88**, 022908 (2013).
[17] Y. Rouzaire and D. Levis, Defect superdiffusion and unbinding in a 2D xy model of self-driven rotors, Phys. Rev. Lett. **127**, 088004 (2021).
[18] R. Contractor, W. Noh, W. Redjem, W. Qarony, E. Martin, S. Dhuey, A. Schwartzberg, and B. Kanté, Scalable single-mode surface-emitting laser via open-Dirac singularities, Nature (London) **608**, 692 (2022).
[19] A. Dikopoltsev, T. H. Harder, E. Lustig, O. A. Egorov, J. Beierlein, A. Wolf, Y. Lumer, M. Emmerling, C. Schneider, S. Höfling, M. Segev, and S. Klembt, Topological insulator vertical-cavity laser array, Science **373**, 1514 (2021).
[20] M. A. Bandres, S. Wittek, G. Harari, M. Parto, J. Ren, M. Segev, D. N. Christodoulides, and M. Khajavikhan, Topological insulator laser: Experiments, Science **359**, eaar4005 (2018).
[21] C. A. Rosiek, G. Arregui, A. Vladimirova, M. Albrechtsen, B. Vosoughi Lahijani, R. E. Christiansen, and S. Stobbe, Observation of strong backscattering in Valley-Hall photonic topological interface modes, Nat. Photonics **17**, 386 (2023).
[22] Z. Wang, Y. Chong, J. D. Joannopoulos, and M. Soljačić, Observation of unidirectional backscattering-immune topological electromagnetic states, Nature (London) **461**, 772 (2009).
[23] M. Hafezi, E. A. Demler, M. D. Lukin, and J. M. Taylor, Robust optical delay lines with topological protection, Nat. Phys. **7**, 907 (2011).
[24] V. Pal, C. Tradonsky, R. Chriki, A. A. Friesem, and N. Davidson, Observing dissipative topological defects with coupled lasers, Phys. Rev. Lett. **119**, 013902 (2017).

[25] L. Yang, G. Li, X. Gao, and L. Lu, Topological-cavity surface-emitting laser, Nat. Photonics **16**, 279 (2022).
[26] C. E. Rüter, K. G. Makris, R. El-Ganainy, D. N. Christodoulides, M. Segev, and D. Kip, Observation of parity–time symmetry in optics, Nat. Phys. **6**, 192 (2010).
[27] G. Arwas, S. Gadasi, I. Gershenzon, A. Friesem, N. Davidson, and O. Raz, Anyonic-parity-time symmetry in complex-coupled lasers, Sci. Adv. **8**, eabm7454387 (2022).
[28] M. Nixon, E. Ronen, A. A. Friesem, and N. Davidson, Observing geometric frustration with thousands of coupled lasers, Phys. Rev. Lett. **110**, 184102 (2013).
[29] Z. Wang, A. Marandi, K. Wen, R. L. Byer, and Y. Yamamoto, Coherent Ising machine based on degenerate optical parametric oscillators, Phys. Rev. A **88**, 063853 (2013).
[30] P. L. McMahon, A. Marandi, Y. Haribara, R. Hamerly, C. Langrock, S. Tamate, T. Inagaki, H. Takesue, S. Utsunomiya, K. Aihara *et al.*, A fully programmable 100-spin coherent Ising machine with all-to-all connections, Science **354**, 614 (2016).
[31] A. Marandi, Z. Wang, K. Takata, R. L. Byer, and Y. Yamamoto, Network of time-multiplexed optical parametric oscillators as a coherent Ising machine, Nat. Photonics **8**, 937 (2014).
[32] C. Tradonsky, I. Gershenzon, V. Pal, R. Chriki, A. Friesem, O. Raz, and N. Davidson, Rapid laser solver for the phase retrieval problem, Sci. Adv. **5**, eaax4530 (2019).
[33] A. Pando, S. Gadasi, A. Friesem, and N. Davidson, Improved laser phase locking with intra-cavity adaptive optics, Opt. Express **31**, 6947 (2023).
[34] C. Tradonsky, S. Mahler, G. Cai, V. Pal, R. Chriki, A. A. Friesem, and N. Davidson, High-resolution digital spatial control of a highly multimode laser, Optica **8**, 880 (2021).
[35] H. Cao, R. Chriki, S. Bittner, A. A. Friesem, and N. Davidson, Complex lasers with controllable coherence, Nat. Rev. Phys. **1**, 156 (2019).
[36] J. Arnaud, Degenerate optical cavities, Appl. Opt. **8**, 189 (1969).
[37] C. Tradonsky, V. Pal, R. Chriki, N. Davidson, and A. A. Friesem, Talbot diffraction and Fourier filtering for phase locking an array of lasers, Appl. Opt. **56**, A126 (2017).
[38] J. R. Leger, Lateral mode control of an AlGaAs laser array in a Talbot cavity, Appl. Phys. Lett. **55**, 334 (1989).
[39] S. S. Cohen, V. Eckhouse, A. A. Friesem, and N. Davidson, Single frequency lasing using coherent combining, Opt. Commun. **282**, 1861 (2009).
[40] M. Fridman, M. Nixon, E. Ronen, A. A. Friesem, and N. Davidson, Phase locking of two coupled lasers with many longitudinal modes, Opt. Lett. **35**, 526 (2010).
[41] P. Smith, Stabilized, single-frequency output from a long laser cavity, IEEE J. Quantum Electron. **1**, 343 (1965).
[42] See Supplemental Material at http://link.aps.org/supplemental/10.1103/PhysRevLett.133.113803 for detailed experimental arrangement, equations derivations, and additional experimental results.
[43] L. Mandel and E. Wolf, Coherence properties of optical fields, Rev. Mod. Phys. **37**, 231 (1965).
[44] A. T. Friberg and R. J. Sudol, The spatial coherence properties of Gaussian Schell-model beams, Opt. Acta **30**, 1075 (1983).
[45] D. Witthaut and M. Timme, Kuramoto dynamics in Hamiltonian systems, Phys. Rev. E **90**, 032917 (2014).
[46] S. Longhi, Non-Hermitian laser arrays with tunable phase locking, Opt. Lett. **47**, 2040 (2022).
[47] V. Pal, S. Mahler, C. Tradonsky, A. A. Friesem, and N. Davidson, Rapid fair sampling of the xy spin Hamiltonian with a laser simulator, Phys. Rev. Res. **2**, 033008 (2020).
[48] R. Chriki, S. Mahler, C. Tradonsky, V. Pal, A. A. Friesem, and N. Davidson, Spatiotemporal supermodes: Rapid reduction of spatial coherence in highly multimode lasers, Phys. Rev. A **98**, 023812 (2018).
[49] F. Rogister, K. S. Thornburg Jr, L. Fabiny, M. Möller, and R. Roy, Power-law spatial correlations in arrays of locally coupled lasers, Phys. Rev. Lett. **92**, 093905 (2004).
[50] M. Honari-Latifpour and M.-A. Miri, Mapping the xy Hamiltonian onto a network of coupled lasers, Phys. Rev. Res. **2**, 043335 (2020).
[51] S. H. Strogatz and R. E. Mirollo, Collective synchronisation in lattices of nonlinear oscillators with randomness, J. Phys. A **21**, L699 (1988).
[52] H. Sakaguchi, S. Shinomoto, and Y. Kuramoto, Local and global self-entrainments in oscillator lattices, Prog. Theor. Phys. **77**, 1005 (1987).